IEEE Open Journal of Vehicular Technology

Received 9 April 2026; accepted 24 April 2026. Date of publication 28 April 2026;
date of current version 20 May 2026. The review of this article was coordinated by Editor Sarbajit Paul.

Digital Object Identifier 10.1109/OJVT.2026.3688077

Fixed-Time Constraint-Aware Sliding-Mode Control for Ride Comfort Enhancement in Active Vehicle Suspensions

RACHID FATTAH [1] (Member, IEEE), JEAN-PIERRE KENNÉ [2], KHALID BENJELLOUN [3], AND AHMED CHEBAK [1] (Senior Member, IEEE)

Green Tech Institute, Mohammed VI Polytechnic University (UM6P), Ben Guerir 43150, Morocco
Department of Mechanical Engineering, École de Technologie Supérieure, Montreal, QC H3C 1K3, Canada
École Mohammadia d'Ingénieurs, Mohammed V University, Rabat B.P. 765, Morocco

CORRESPONDING AUTHOR: Rachid Fattah (e-mail: rachid.fattah@um6p.ma).

ABSTRACT Active vehicle suspensions must improve ride comfort while respecting strict suspension-travel and tire-load constraints under uncertain road disturbances. Although sliding-mode control ensures robustness, conventional designs provide only asymptotic convergence and may generate chattering, limiting transient predictability and practical implementation. This paper proposes a continuous, non-singular fixed-time sliding-mode controller (FxT–SMC) with explicit constraint awareness for nonlinear quarter-car active suspensions. A state-dependent sliding map guarantees fixed-time convergence with an initial-condition-independent settling-time bound, while a smooth reciprocal barrier embedded in the sliding surface enforces forward invariance of the admissible travel set without discontinuous projection. Global fixed-time stability and bounded zero dynamics are rigorously established via Lyapunov analysis. Experimental validation over representative road profiles demonstrates predictable sub–2-second transients, strict satisfaction of travel and tire-load limits, and significant improvements in ISO 2631-1 comfort metrics compared with passive suspension, classical SMC, and super-twisting control. The results highlight the effectiveness of fixed-time, constraint-aware sliding-mode control for practical intelligent active suspension systems.

INDEX TERMS Active suspension systems, fixed-time stability, nonlinear control systems, ride comfort, sliding-mode control, vehicular technology.

I. INTRODUCTION

Active vehicle suspension systems (AVSS) are a primary lever for improving ride comfort, road-holding capability, and overall vehicular stability, as actuators can inject or dissipate energy in real time to counteract road-induced vibrations [1], [2], [3], [4]. Compared with passive suspensions, active architectures must simultaneously satisfy human-centric comfort criteria, enforce strict physical bounds on suspension deflection and tire load, and operate within actuator limitations under uncertain and time-varying road disturbances. Recent studies report significant progress in robustness enhancement, constraint handling, and implementation realism for nonlinear quarter-car and half-car platforms [2], [3], [5], [6], [7], [8], [9]. These developments underscore the need for controllers capable of delivering smooth actuation signals [10], predictable transient responses, and verifiable comfort gains under representative and standardized road profiles [11].

Sliding-mode control (SMC) remains a natural and widely adopted candidate owing to its intrinsic robustness against matched uncertainties and external disturbances [12], [13], [14]. Nevertheless, two structural limitations restrict its suitability for time-critical vehicular suspension tasks. First, classical SMC guarantees only asymptotic convergence, providing no uniform upper bound on settling time. Second, discontinuous switching may induce high-frequency chattering, which propagates to actuator dynamics and manifests as spike-like transients in weighted acceleration signals [15], [16]. To mitigate these issues, the literature has explored modified reaching laws, disturbance observers [17], [18], output-feedback and intelligent augmentations [19], [20],

[21], and saturation-aware formulations [15], [16], [22], [23], [24]. Recent vibration-control designs further exploit actuator saturation and structural nonlinearities to balance comfort and energy use [25], [26], and address reliability through fault-tolerant strategies under partial measurements [27]. Model-free finite-time regulation with input saturation and dead zones has also emerged, together with energy-regenerative considerations and preview information, to better reflect implementation constraints [28], [29].

Fixed-time stability (FxTS) offers a structurally stronger convergence framework by ensuring a *uniform* upper bound on the settling time that is independent of the initial state [30], [31], [32], [33]. Such predictability is particularly attractive in automotive applications, where transient duration directly impacts passenger comfort, constraint satisfaction, and safety margins. Within suspension control, finite- and fixed-time approaches have therefore gained traction for coping with nonlinearities, actuator limits, and unmodeled dynamics [34], [35], [36]. However, several open challenges remain: avoiding singular behavior near the origin, reducing discontinuities in the equivalent control, enforcing suspension-travel and tire-load limits without hard switching mechanisms, and validating performance using human-oriented comfort metrics under realistic road excitations [37], [38]. These limitations reveal a gap between fixed-time control theory and practically implementable vehicular suspension strategies. Recent works have also explored constraint-aware vehicle modeling using discrete constraint formulations [39] and barrier-function-based sliding-mode control for automotive systems such as active anti-roll control [40]. However, these approaches address different system configurations and do not explicitly combine fixed-time convergence with constraint-aware sliding-mode control for active suspension systems.

This work: We propose a continuous, non-singular fixed-time sliding-mode controller (FxT–SMC) for a nonlinear quarter-car model with matched disturbances and explicit physical constraints. The design employs a state-dependent nonlinear exponent in the sliding map to establish global fixed-time convergence while avoiding singularities [31]. In addition, a smooth reciprocal barrier function is embedded directly into the sliding surface to penalize the approach to suspension-deflection limits, thereby ensuring forward invariance of the admissible set without discontinuous projection or hybrid switching logic. In contrast to classical SMC and super-twisting algorithms (STA), the resulting feedback structure dispenses with abrupt switching in the equivalent control, which contributes to mitigating chattering and suppressing crest-factor amplification in the weighted acceleration signal. This unified structure jointly addresses convergence-time certification, constraint preservation, and smooth implementability within a single analytical framework.

Scope and evaluation protocol: The controller is assessed on a comprehensive set of representative road inputs—periodic excitation, filtered random profile, localized defects (pothole and bump), step-like disturbances, and broadband frequency sweeps—so as to probe both low-frequency body motion and band-limited resonant effects that dominate perceived discomfort. Performance is quantified via ISO 2631-1 indicators (RMS, VDV, and crest factor) [37], [38], body-position tracking RMSE, and strict verification of suspension-travel and tire-load bounds, alongside analysis of control smoothness. Comparative baselines include passive suspension as well as classical SMC and super-twisting algorithms [12], [13], [15]. Particular emphasis is placed on transient predictability: fixed-time reaching and on-manifold decay are jointly established in Lyapunov form, yielding a uniform convergence guarantee that does not depend on initial-condition tuning.

Contributions: The paper makes three principal contributions: (i) a continuous, constraint-aware FxT–SMC framework that couples fixed-time reaching with fixed-time on-manifold decay under matched disturbances; (ii) a barrier-shaped sliding surface that enforces suspension-travel limits through forward invariance while maintaining smooth, non-singular feedback; and (iii) a systematic theoretical and experimental evaluation on diverse road profiles using ISO comfort metrics and safety constraints, demonstrating predictable transients, reduced chattering, and robustness to initial-condition variations within a unified vehicular control framework.

Organization of the paper: Section II recalls fixed-time stability notions and the Lyapunov criterion used in the analysis. Section III formulates the nonlinear quarter-car model, states the *Modeling Assumptions*, and specifies the *Performance Objectives and Constraints* (suspension travel, tire load, tracking, and ISO comfort metrics). Section IV presents the robust, constraint-aware FxT–SMC design, including the state-dependent sliding map, the reciprocal-barrier shaping, the Lyapunov proof of global fixed-time convergence, and the *Zero Dynamics Analysis*. Section V details the test bench and parameters, the controller setup and road profiles, and reports the *Performance Evaluation* and the *Robustness Evaluation* with respect to initial conditions. Finally, Section VI summarizes the main findings and outlines future work.

II. PRELIMINARIES

This section briefly recalls fixed-time stability (FTS) theory, which underpins the proposed controller's convergence guarantees.

A. STABILITY DEFINITIONS AND CRITERION

Consider the autonomous system

$$\dot{x} = f(x), \qquad x(0) = x_0, \qquad x \in \mathbb{R}^n, \tag{1}$$

with continuous f and $f(0) = 0$.

Finite-Time Stability (FTS) [41], [42]: There exists a continuous *settling-time function* $\mathcal{T}(x_0) > 0$ such that the solution satisfies $x(t) = 0$ for all $t \geq \mathcal{T}(x_0)$.

Fixed-Time Stability (FxTS) [30]: There exists a *uniform bound* $\mathcal{T}_u > 0$ such that $\mathcal{T}(x_0) \leq \mathcal{T}_u$ for all initial states x_0.

We use the following Lyapunov criterion.

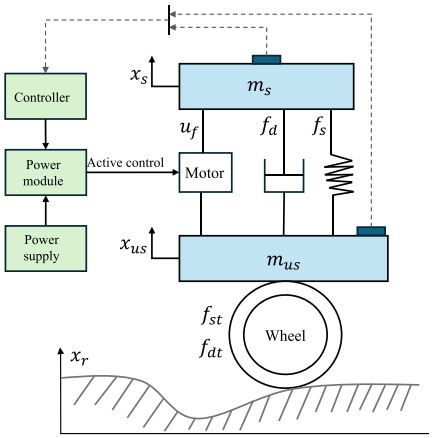

FIGURE 1. Nonlinear quarter active suspension system.

Lemma II.1 (Fixed-Time Criterion [30], [43]): Let $\mathcal{U}(x) > 0$ be C^1. If

$$\dot{\mathcal{U}}(x) \le -c_1\mathcal{U}^p - c_2\mathcal{U}^q, \tag{2}$$

with $c_1, c_2 > 0$, $0 < p < 1 < q$, then the origin is globally fixed-time stable and

$$\mathcal{T}_u \le \frac{1}{c_1(1-p)} + \frac{1}{c_2(q-1)}. \tag{3}$$

B. FIXED-TIME SLIDING MODE STRUCTURE

Consider the second-order system with matched disturbance:

$$\dot{x}_1 = x_2, \quad \dot{x}_2 = F(x) + G(x)\,u + \Delta(t), \tag{4}$$

where F, G are smooth, $G(x) \neq 0$, and $|\Delta(t)| \le \delta$.

Define the sliding variable

$$\sigma = x_2 + \kappa\,\psi(x_1), \tag{5}$$

where $\kappa > 0$, and the non-singular state-dependent map

$$\psi(x_1) = |x_1|^{\frac{ax_1^2}{1+bx_1^2}}\ \mathrm{sgn}(x_1), \tag{6}$$

with shape parameters $a, b > 0$.

On $\sigma = 0$, the reduced dynamics read

$$\dot{x}_1 = -\kappa\,\psi(x_1), \tag{7}$$

which are globally fixed-time stable [31]. In particular,

Lemma II.2 (FxTS with non-constant exponent [31]): Let $\vartheta = \frac{a}{1+b}$. Then the settling-time bound satisfies

$$\mathcal{T}_u \le \frac{1}{\kappa(\vartheta-1)} + \frac{1}{\kappa e^{-a/(2e)}}. \tag{8}$$

III. PROBLEM STATEMENT

We consider a nonlinear quarter-car model with sprung mass m_s and unsprung mass m_{us}, vertical displacements x_s, x_{us}, and road excitation x_r. The actuator force is u, and the suspension spring and damper forces are f_s, f_d, respectively. See Fig. 1.

The equations of motion are:

$$\begin{cases} m_s\ddot{x}_s + f_s + f_d - u = 0 \\ m_{us}\ddot{x}_{us} + f_t - f_s - f_d + u = 0 \end{cases} \tag{9}$$

Spring and damping forces include nonlinearities:

$$f_s = k_1(x_s - x_{us}) + k_2\beta_1(x_s - x_{us})^3 \tag{10}$$

$$f_d = c_1(\dot{x}_s - \dot{x}_{us}) + c_2\beta_2(\dot{x}_s - \dot{x}_{us})^2 \tag{11}$$

Tire-road interaction is:

$$f_t = f_{st} + f_{dt}, \quad f_{st} = k_t(x_{us} - x_r), \quad f_{dt} = c_t(\dot{x}_{us} - \dot{x}_r) \tag{12}$$

Defining the state vector:

$$x = \begin{bmatrix} x_1 & x_2 & x_3 & x_4 \end{bmatrix}^T = \begin{bmatrix} x_s & \dot{x}_s & x_{us} & \dot{x}_{us} \end{bmatrix}^T$$

and introducing a bounded lumped disturbance $\Delta(t)$ acting on the sprung mass, the control-oriented model becomes:

$$\begin{cases} \dot{x}_1 &= x_2, \\ \dot{x}_2 &= \frac{1}{m_s}(-f_s - f_d + u) + \Delta(t), \\ \dot{x}_3 &= x_4, \\ \dot{x}_4 &= \frac{1}{m_{us}}(f_s + f_d - f_t - u). \end{cases} \tag{13}$$

A. MODELING ASSUMPTIONS

In the remainder of this paper, we make the following assumptions regarding the external disturbance and road input:

Assumption III.1: The lumped (matched) disturbance acting on the sprung mass is bounded; that is, there exists a known constant $\delta > 0$ such that

$$|\Delta(t)| \le \delta \quad \text{for all } t \ge 0.$$

Assumption III.2: The road excitation signal $x_r(t)$ and its first derivative $\dot{x}_r(t)$ are bounded for all $t \ge 0$, i.e., there exist constants $\bar{x}_r$, $\bar{v}_r > 0$ such that:

$$|x_r(t)| \le \bar{x}_r, \quad |\dot{x}_r(t)| \le \bar{v}_r.$$

Remark III.1: The above assumptions are essential for the stability analysis and, in particular, for the applicability of the fixed-time convergence results established in Lemma 2.1 and Lemma 2.2. The boundedness of the road excitation and its derivative ensures that the lumped disturbance entering the system remains bounded, which is a key requirement for guaranteeing the reaching condition and the fixed-time stability of the sliding dynamics.

From a closed-loop perspective, these assumptions directly affect the internal (zero) dynamics through the input term $Q(t)$, which depends on $x_r(t)$, $\dot{x}_r(t)$, and $\Delta(t)$. When these signals are bounded, the internal dynamics correspond to a stable linear system driven by a bounded input, ensuring that the state remains bounded, as established in Proposition 4.1.

If these assumptions are violated, for instance in the presence of unbounded or highly irregular disturbances, the term $Q(t)$ may no longer be bounded. In such a case, the internal

TABLE 1. ISO 2631-1 Comfort Classification Thresholds

Comfort Level	$a_{w,\mathrm{RMS}}$ (m/s^2)	VDV (m/s$^{1.75}$)	CF
Very Comfortable	< 0.315	< 8	< 9
Comfortable	0.315–0.63	8–9	9–10
Acceptable	0.63–1.0	9–10	10–12
Uncomfortable	1.0–1.6	10–12	12–14
Very Uncomfortable	1.6–2.5	12–15	14–16
Extremely Uncomfortable	> 2.5	> 15	> 16

dynamics may exhibit unbounded trajectories, and the fixed-time convergence guarantees derived in the stability analysis may no longer strictly hold.

Nevertheless, in practical suspension systems, road excitations and their rates of variation are inherently bounded due to physical constraints, which makes these assumptions reasonable for real-world implementations.

B. PERFORMANCE OBJECTIVES AND CONSTRAINTS

The active suspension system aims to: (i) enhance ride comfort, (ii) limit suspension deflection, (iii) preserve tire-road contact, and (iv) ensure vertical tracking of the body. These objectives are detailed below:

- *Suspension deflection:* Let the signed suspension travel be $\zeta := x_s - x_{us}$ and its magnitude $z := |\zeta|$. The travel constraint is

$$z \le z_r, \tag{14}$$

  where $z_r > 0$ denotes the maximum admissible suspension travel. For later use, we also define the normalized travel $w := \zeta / z_r \in (-1, 1)$.
- *Tire dynamic load:* To ensure road contact, the tire force must remain bounded by:

$$|f_t| \le (m_s + m_{us})g \tag{15}$$

- *Tracking accuracy:* The root mean square error (RMSE) of the sprung mass position is given by:

$$\mathrm{RMSE}_x = \sqrt{\frac{1}{T}\int_0^T (x_s(t) - x_{\mathrm{ref}}(t))^2 \, dt} \tag{16}$$

- *Ride comfort:* Minimize the vertical acceleration $\ddot{x}_s$ transmitted to passengers. This is evaluated using ISO 2631-1 comfort indicators.
  The ISO 2631-1 comfort classification thresholds used in this study are summarized in Table 1.

To evaluate ride comfort under vertical vibrations, ISO 2631-1 [37] recommends frequency-weighted acceleration indicators, also adopted in [2]. These include:

- *Weighted RMS Acceleration ($a_{w,RMS}$):*

$$a_{w,\mathrm{RMS}} = \sqrt{\frac{1}{T}\int_0^T a_w^2(t)\, dt} \tag{17}$$

  where $a_w(t)$ is the output of the ISO 2631-1 weighting filter $W^{(5)}(s)$ applied to $\ddot{x}_s(t)$.
- *Vibration Dose Value (VDV):*

$$\mathrm{VDV} = \left(\int_0^T a_w^4(t)\, dt\right)^{1/4} \tag{18}$$

- *Crest Factor (CF):*

$$\mathrm{CF} = \frac{\max |a_w(t)|}{a_{w,\mathrm{RMS}}} \tag{19}$$

The frequency weighting filter used in this study follows the fifth-order transfer function from [37]:

$$W^{(5)}(s) = \frac{N(s)}{D(s)}, \tag{20}$$

where $N(s)$ and $D(s)$ are 4th- and 5th-order polynomials defined in [37].

This filter mimics the human body's sensitivity to whole-body vibration in the 4–8 Hz range. The resulting $a_w(t)$ signal is used in computing the ISO comfort metrics.

IV. ROBUST FIXED-TIME CONTROL DESIGN

This section presents the design of a robust fixed-time sliding mode controller (FxT-SMC) for the nonlinear quarter-car suspension system. The control objective is to ensure that the vertical displacement of the sprung mass, denoted $x_1(t)$, converges to the equilibrium position in a fixed time, regardless of the initial condition and in the presence of matched bounded disturbances.

A. SYSTEM REPRESENTATION

We consider the simplified second-order dynamics governing the motion of the sprung mass:

$$\begin{cases} \dot{x}_1 &= x_2, \\ \dot{x}_2 &= F(x) + G(x)\, u + \Delta(t), \end{cases} \tag{21}$$

where

- $x_1 = x_s$, $x_2 = \dot{x}_s$: displacement and velocity of the sprung mass,
- $u(t)$: control input (actuator force),
- $F(x) = \frac{1}{m_s}[-f_s(x) - f_d(x)]$,
- $G(x) = \frac{1}{m_s}$,
- $\Delta(t)$: matched disturbance, with $|\Delta(t)| \le \delta$.

B. SLIDING SURFACE AND CONTROL LAW

We adopt the nonlinear sliding surface

$$\sigma(x) = x_2 + \kappa\, \psi(x_1), \tag{22}$$

with $\kappa > 0$ and

$$\psi(x_1) = |x_1|^{\frac{ax_1^2}{1+bx_1^2}} \operatorname{sgn}(x_1), \qquad a, b > 0. \tag{23}$$

Remark IV.1: Although the analytical expression of the derivative of $\psi(x_1)$ involves the term $\ln|x_1|$, which is not defined at $x_1 = 0$, this does not introduce a singularity in the control law. Indeed, it holds that

$$\lim_{x_1 \to 0} |x_1| \ln |x_1| = 0,$$

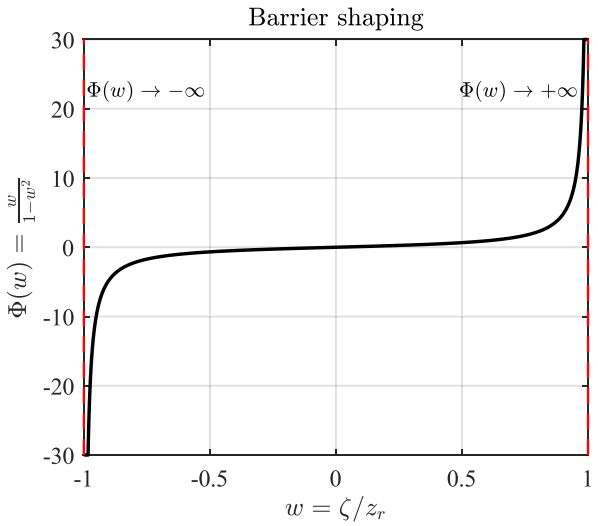

FIGURE 2. Barrier shaping $\Phi(w) = \frac{w}{1-w^2}$ for the normalized travel $w = \zeta/z_r$. The map is smooth on $(-1, 1)$ and unbounded as $w \to \pm 1$, enforcing a soft approach to the travel limits.

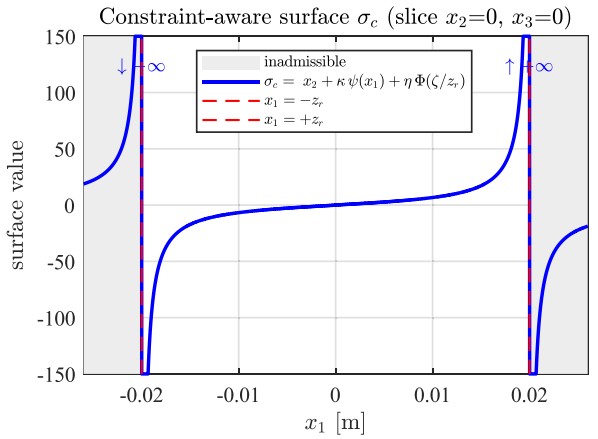

FIGURE 3. Constraint-aware surface $\sigma_c = x_2 + \kappa\,\psi(x_1) + \eta\,\Phi(\zeta/z_r)$ on the slice $x_2 = 0$, $x_3 = 0$ (with $z_r = 0.02$ m). Vertical dashed lines mark $x_1 = \pm z_r$; the barrier term steepens the surface near the limits.

which implies that the nonlinear terms defining $\psi(x_1)$ remain bounded and continuous at the origin. As a result, the sliding map $\psi(x_1)$ is well-defined on $\mathbb{R}$, and the closed-loop system remains non-singular.

To encode the suspension travel constraint, let the signed travel be $\zeta := x_1 - x_3$ and its normalized form $w := \zeta/z_r \in (-1, 1)$. We augment the surface with the smooth reciprocal barrier $\Phi(w) = \frac{w}{1-w^2}$ and use the constraint-aware surface

$$\sigma_c(x) \;=\; \sigma(x) \;+\; \eta\,\Phi\!\left(\frac{\zeta}{z_r}\right), \qquad \eta > 0. \tag{24}$$

As illustrated in Fig. 2, $\Phi(w)$ is smooth on $(-1, 1)$ and diverges as $|w| \to 1$, which naturally penalizes the approach to the travel limits. On the 2-D slice $x_2 = 0$, $x_3 = 0$ (Fig. 3), the resulting σ_c steepens near $x_1 = \pm z_r$, guiding trajectories away from constraint violation while keeping the feedback finite on

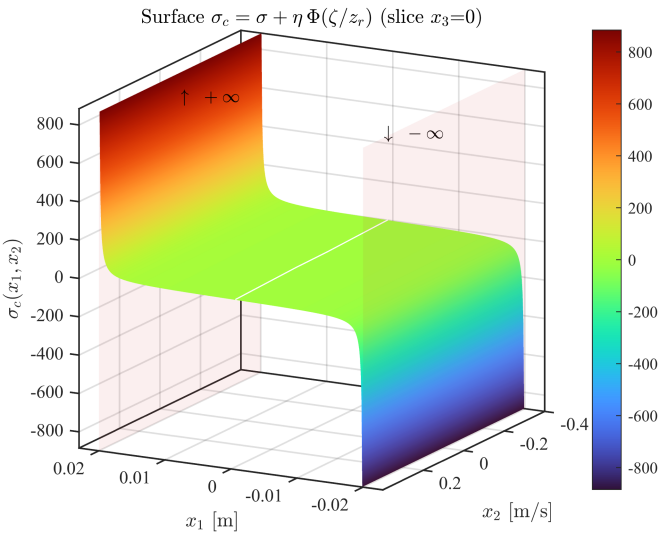

FIGURE 4. Surface $\sigma_c(x_1, x_2) = x_2 + \kappa\,\psi(x_1) + \eta\,\Phi(\zeta/z_r)$ on the slice $x_3 = 0$ with $z_r = 0.02$ m and $\eta = 10$. Vertical translucent planes mark $x_1 = \pm z_r$; the barrier creates steep ridges as $|\zeta|/z_r \to 1$, which push trajectories away from the travel limits.

the admissible set. The full surface $\sigma_c(x_1, x_2)$ for $x_3 = 0$ is shown in Fig. 4, where the ridges close to $|x_1| = z_r$ visualize the barrier's effect in three dimensions.

A. Influence of the barrier term on the reaching phase: In addition to enforcing the suspension travel constraint through forward invariance, the barrier function $\Phi(w)$ also influences the reaching phase dynamics. Since the sliding variable is defined as $\sigma_c = \sigma + \eta\Phi(w)$, its time derivative explicitly contains the term $\eta\Phi'(w)\dot{w}$, which contributes to the evolution of σ_c before the sliding manifold is reached.

As the normalized travel w approaches its admissible limits, the barrier term introduces a state-dependent corrective action that modifies the direction of the vector field and prevents trajectories from approaching the constraint boundary. This effect is already active during the reaching phase and reshapes the convergence dynamics toward the sliding manifold.

Therefore, the barrier function does not only ensure constraint satisfaction during the sliding motion, but also actively participates in the reaching phase by influencing the transient behavior of σ_c while preserving the fixed-time convergence property. Based on (24), the proposed control law is

$$\begin{aligned} u(x) = \; & -\,G^{-1}(x)\Big(F(x) + \ell_1\,\mathrm{sgn}(\sigma_c) + \ell_2\,|\sigma_c|^{\rho}\,\mathrm{sgn}(\sigma_c) \\ & + \kappa\,\frac{a\,|x_1|\,x_2}{1+bx_1^2}\left(1 + \frac{2\ln|x_1|}{1+bx_1^2}\right)|x_1|^{\frac{ax_1^2}{1+bx_1^2}} \\ & + \eta\,\frac{1+w^2}{(1-w^2)^2}\,\frac{x_2 - x_4}{z_r}\Big). \end{aligned} \tag{25}$$

where $\ell_1 > \delta$, $\ell_2 > 0$, and $\rho > 1$ are design gains.

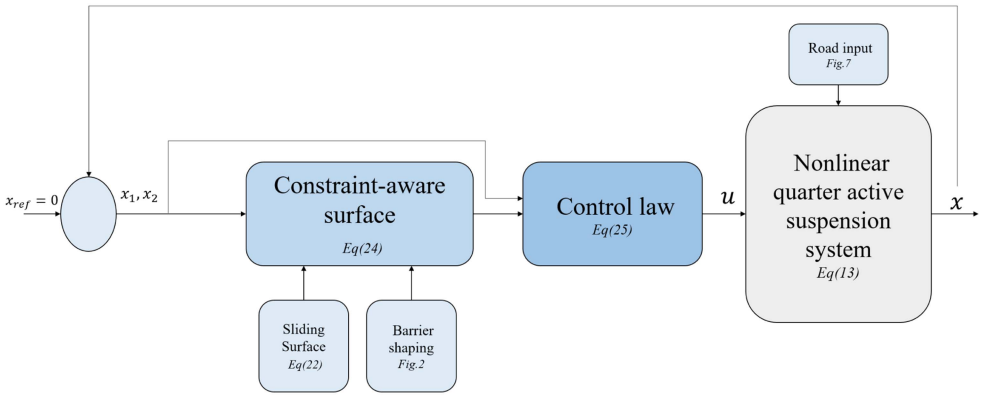

FIGURE 5. Block diagram of the proposed constraint-aware fixed-time sliding-mode control scheme.

B. Interpretation of the control law: The control law in (25) combines several nonlinear components that jointly ensure robustness, constraint enforcement, and fixed-time convergence.

The discontinuous term $\ell_1\,\mathrm{sgn}(\sigma_c)$ guarantees robustness against bounded disturbances and enforces a strict reaching condition for the sliding variable. The nonlinear term $\ell_2\,|\sigma_c|^{\rho}\,\mathrm{sgn}(\sigma_c)$, with $\rho > 1$, introduces a higher-order dissipation mechanism that is essential to achieve fixed-time convergence according to Lemma 2.1.

The term associated with $\psi(x_1)$ governs the nonlinear sliding dynamics and ensures fixed-time convergence of the state during the sliding phase, as established by Lemma 2.2. In addition, the barrier-related term involving $\Phi(w)$ enforces the suspension travel constraint while contributing to the evolution of the sliding variable.

Overall, these terms define a unified control structure in which the reaching phase and the sliding phase are both governed by fixed-time mechanisms, resulting in a uniform convergence bound for the complete closed-loop system.

Fig. 5 illustrates the overall structure of the proposed constraint-aware fixed-time sliding-mode control scheme.

C. STABILITY ANALYSIS AND MAIN RESULT

Theorem 1 (Global Fixed-Time Stability): Consider the system (21) controlled by (25) with sliding surface (24). Assume: (i) $G(x) = 1/m_s > 0$ and $F(x)$ is locally Lipschitz; (ii) the disturbance is bounded $|\Delta(t)| \le \delta$; and (iii) the gains satisfy $\ell_1 > \delta$, $\ell_2 > 0$, $\rho > 1$, $\kappa > 0$, $a > 0$, $b > 0$, $\eta > 0$. Then the closed-loop system is globally fixed-time stable with respect to $x_1(t)$, and the total uniform settling-time bound satisfies

$$T^{\star} \le \frac{1}{\ell_1 - \delta} + \frac{1}{\ell_2(\rho - 1)} + \frac{1}{\kappa(\vartheta - 1)} + \frac{1}{\kappa e^{-a/(2e)}},$$
$$\vartheta = \frac{a}{1+b}. \tag{26}$$

Moreover, if $|w(0)| < 1$, then $|w(t)| < 1$ for all $t \ge 0$.

Before proceeding with the proof, it is useful to emphasize that the convergence analysis is performed in two successive stages. The first stage corresponds to the reaching phase, during which the constraint-aware sliding variable σ_c converges to zero in fixed time. The second stage corresponds to the sliding phase, during which the state x_1 converges to the equilibrium along the manifold $\sigma_c = 0$. The overall settling time is therefore obtained by combining the upper bounds associated with these two stages.

Proof:

Step 1. Reaching phase: Let $W(\sigma_c) = \sigma_c^2$. By direct differentiation of (24) and (21), one gets

$$\dot{\sigma}_c = F(x) + G(x)u + \Delta(t) + \kappa\,\dot{\psi}(x_1) + \eta\,\Phi'(w)\,\dot{w}.$$

From Appendix A, the terms $\dot{\psi}(x_1)$ and $\Phi'(w)\dot{w}$ are explicitly given. Using these expressions, the control law (25) can be rewritten as

$$u(x) = -G^{-1}(x)\big(F(x) + \ell_1\mathrm{sgn}(\sigma_c) + \ell_2|\sigma_c|^{\rho}\mathrm{sgn}(\sigma_c) + \kappa\dot{\psi}(x_1) + \eta\Phi'(w)\dot{w}\big).$$

Substituting into $\dot{\sigma}_c$ yields

$$\begin{aligned}\dot{\sigma}_c &= F(x) + G(x)u(x) + \Delta(t) + \kappa\dot{\psi}(x_1) + \eta\Phi'(w)\dot{w}\\ &= F(x) - \big(F(x) + \ell_1\mathrm{sgn}(\sigma_c) + \ell_2|\sigma_c|^{\rho}\mathrm{sgn}(\sigma_c) + \kappa\dot{\psi}(x_1)\\ &\quad + \eta\Phi'(w)\dot{w}\big) + \Delta(t) + \kappa\dot{\psi}(x_1) + \eta\Phi'(w)\dot{w}.\end{aligned}$$

Hence, the terms $F(x)$, $\kappa\dot{\psi}(x_1)$, and $\eta\Phi'(w)\dot{w}$ cancel exactly, leading to

$$\dot{\sigma}_c = -\ell_1\mathrm{sgn}(\sigma_c) - \ell_2|\sigma_c|^{\rho}\mathrm{sgn}(\sigma_c) + \Delta(t).$$

Therefore,

$$\begin{aligned}\dot{W} &= 2\sigma_c\dot{\sigma}_c \le -2(\ell_1 - \delta)|\sigma_c| - 2\ell_2|\sigma_c|^{\rho+1}.\\ \dot{W} &\le -a_0 W^{1/2} - b_0 W^{(\rho+1)/2},\\ a_0 &= 2(\ell_1 - \delta), \quad b_0 = 2\ell_2.\end{aligned}$$

This inequality matches Lemma 2.1 with

$$p = \frac{1}{2}, \qquad q = \frac{\rho+1}{2}.$$

Hence, the reaching phase is fixed-time stable and satisfies

$$T_s^\star \le \frac{1}{\ell_1 - \delta} + \frac{1}{\ell_2(\rho - 1)}, \qquad \sigma_c(t) \to 0.$$

Step 2. Sliding phase: Once the manifold $\sigma_c = 0$ is reached, the closed-loop dynamics evolve on the sliding set. In this case,

$$x_2 = -\kappa\, \psi(x_1) - \eta\, \Phi(w),$$

and therefore

$$\dot{x}_1 \;=\; -\kappa\, \psi(x_1) \;-\; \eta\, \Phi(w).$$

By comparison, the scalar auxiliary system

$$\dot{z} = -\kappa\, \psi(z)$$

upper-bounds the decay of $|x_1(t)|$. By Lemma 2.2, this reduced dynamics is globally fixed-time stable with the bound

$$T_{x_1}^\star \le \frac{1}{\kappa(\vartheta - 1)} + \frac{1}{\kappa e^{-a/(2e)}}, \qquad \vartheta = \frac{a}{1+b}.$$

The total convergence time is obtained by combining the upper bounds associated with the reaching and sliding phases. More precisely,

$$T^\star \le T_s^\star + T_{x_1}^\star.$$

It is important to note that this decomposition does not require a strict sequential separation between the reaching and sliding phases. The above expression provides a conservative upper bound on the total settling time. In practice, partial overlap between the two phases may occur, leading to faster convergence than the theoretical estimate.

This ensures that the fixed-time property is preserved for the overall closed-loop system, since both phases admit uniform upper bounds independent of the initial condition.

Finally, forward invariance of $|w| < 1$ follows by contradiction. If $|w| \to 1$, then $\Phi(w) \to \pm\infty$, and thus

$$|\sigma_c| = |x_2 + \kappa\psi(x_1) + \eta\Phi(w)|$$

would become unbounded, which contradicts the monotone decay of $W(\sigma_c)$ established in Step 1. Hence, $|w(t)| < 1$ for all $t \ge 0$ whenever $|w(0)| < 1$.

Discussion on admissible initial conditions: It is important to emphasize that the forward invariance property holds under the condition $|w(0)| < 1$, which corresponds to an initial suspension deflection within the admissible physical range. In practical suspension systems, this condition is naturally satisfied due to mechanical constraints that limit the suspension travel. Therefore, the proposed control law operates within a physically meaningful domain of initial conditions.

D. ZERO DYNAMICS ANALYSIS

While the proposed controller (25) ensures the fixed-time convergence of the vertical displacement of the sprung mass $x_1(t)$, it is also necessary to analyze the stability of the internal unsprung dynamics, i.e., the so-called *zero dynamics*, which correspond to the evolution of $x_3(t)$ and $x_4(t)$ under the constraint $x_1(t) \equiv 0$. In the standard output-based sense, we take $y := x_1$ and interpret this analysis along the sliding manifold $\{\sigma_c(x) = 0\}$ induced by the controller (see Section IV).

The effect of external perturbations on the internal dynamics is explicitly captured through the input term $Q(t)$, which reflects the interaction between road excitation and the lumped disturbance acting on the suspension system.

From the full suspension dynamics, setting $x_1 = 0$, the resulting zero dynamics can be written in compact form as:

$$\dot{\chi} = P\chi + Q(t), \tag{27}$$

where $\chi = [x_3\ x_4]^\top$, and

$$P = \begin{bmatrix} 0 & 1 \\ -\frac{k_t}{m_{us}} & -\frac{c_t}{m_{us}} \end{bmatrix}, \tag{28}$$

$$Q(t) = \begin{bmatrix} 0 \\ \frac{k_t x_r(t) + c_t \dot{x}_r(t) + \Delta(t)}{m_{us}} \end{bmatrix}. \tag{29}$$

Proposition IV.1 (Boundedness of the Zero Dynamics): Assume that Assumptions 3.1 and 3.2 hold, and that $k_t > 0$, $c_t > 0$, and $m_{us} > 0$. Then, the internal dynamics governed by (27) are globally bounded for all $t \ge 0$.

Proof: Consider the Lyapunov function $V_\chi = \chi^\top\chi = x_3^2 + x_4^2$. Its derivative along trajectories of (27) yields:

$$\dot{V}_\chi = \dot{\chi}^\top\chi + \chi^\top\dot{\chi} = \chi^\top(P^\top + P)\chi + 2\chi^\top Q(t).$$

The matrix P depends on the physical parameters k_t, c_t, and m_{us}, and is given by

$$P = \begin{bmatrix} 0 & 1 \\ -\frac{k_t}{m_{us}} & -\frac{c_t}{m_{us}} \end{bmatrix}.$$

Under the standard physical conditions $k_t > 0$, $c_t > 0$, and $m_{us} > 0$, the eigenvalues of P lie in the left half-plane, and therefore P is Hurwitz. Consequently, there exists $\lambda_{\min} > 0$ such that:

$$\chi^\top(P^\top + P)\chi \le -\lambda_{\min}\|\chi\|^2.$$

Applying Young's inequality to the cross term, for any $\varepsilon > 0$,

$$2\chi^\top Q(t) \le \frac{1}{\varepsilon}\|\chi\|^2 + \varepsilon\|Q(t)\|^2.$$

Combining terms, we obtain:

$$\dot{V}_\chi \le -\left(\lambda_{\min} - \frac{1}{\varepsilon}\right)\|\chi\|^2 + \varepsilon\|Q(t)\|^2.$$

The boundedness of $Q(t)$ follows directly from its definition. Indeed, $Q(t)$ depends on the road excitation $x_r(t)$, its derivative $\dot{x}_r(t)$, and the lumped disturbance $\Delta(t)$. Under Assumptions 3.2 and 3.1, all these signals are bounded, which implies that there exists a constant $\bar{Q} > 0$ such that

$$\|Q(t)\| \le \bar{Q}, \qquad \forall t \ge 0.$$

TABLE 2. System Parameters

Parameter	Value	Unit
m_s	2.45	kg
m_{us}	1.00	kg
k_{s1}	980	N/m
k_{s2}	100	N/m^3
c_{s1}	7.5	N·s/m
c_{s2}	10	N·s/m
k_t	2500	N/m
c_t	5	N·s/m
β_1, β_2	1	–

It is important to note that the disturbance $\Delta(t)$ enters the zero dynamics as an additive bounded input through $Q(t)$, and does not affect the stability of the homogeneous part of the system. Since the matrix P is Hurwitz, the unforced dynamics are exponentially stable, and the presence of a bounded input results in bounded trajectories.

Moreover, in the presence of moderate parameter uncertainties, the Hurwitz property of P is preserved as long as the parameters remain within physically meaningful ranges. If these conditions are violated, the stability of the internal dynamics may no longer be guaranteed, which reflects a limitation of the model rather than of the control design.

Using the bound on $Q(t)$, we obtain:

$$\dot{V}_\chi \leq -\left(\lambda_{\min} - \frac{1}{\varepsilon}\right)\|\chi\|^2 + \varepsilon\bar{Q}^2.$$

Choosing ε such that $\lambda_{\min} > \frac{1}{\varepsilon}$, we deduce:

$$\dot{V}_\chi \leq -\pi_1 V_\chi + \pi_2,$$

with $\pi_1 = \lambda_{\min} - \frac{1}{\varepsilon} > 0$ and $\pi_2 = \varepsilon\bar{Q}^2 > 0$.

This linear differential inequality implies:

$$V_\chi(t) \leq V_\chi(0)e^{-\pi_1 t} + \frac{\pi_2}{\pi_1}\left(1 - e^{-\pi_1 t}\right) \leq \varpi,$$

for some finite constant $\varpi > 0$. Therefore, both $x_3(t)$ and $x_4(t)$ remain globally bounded.

V. EXPERIMENTAL VALIDATION

A. EXPERIMENTAL SETUP

The proposed FxT–SMC controller was evaluated using a quarter-car active-suspension configuration. The assembly comprises three vertically stacked stages: a top plate (sprung mass), a middle plate (unsprung mass), and a base stage that imposes road profiles via a lead-screw–driven actuator. A DC motor applies the control force between the sprung and unsprung stages. This configuration reproduces the vertical dynamics of a quarter car for assessing the controller. Fig. 6 shows the setup.

The system parameters, used for both simulation and implementation, are summarized in Table 2. They reflect realistic stiffness and damping nonlinearities.

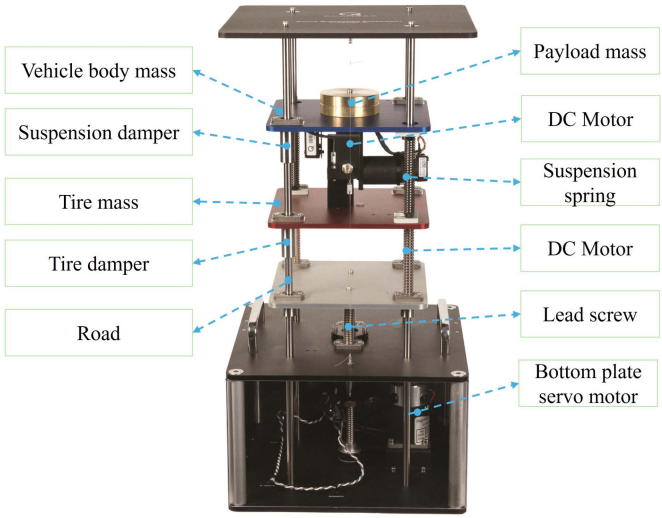

FIGURE 6. Quarter-car suspension platform.

B. CONTROLLER SETUP AND ROAD PROFILES

Four control strategies were implemented:

1) *PS:* Passive suspension (no control);
2) *SMC:* Classical sliding mode control;
3) *STA:* Super-Twisting Algorithm (second-order SMC);
4) *Proposed:* Robust FxT-SMC.

FxT-SMC parameters were selected based on systematic tuning guidelines to ensure a balance between convergence speed, robustness, and control smoothness. In particular, the gain ℓ_1 is chosen to exceed the disturbance bound, ensuring the reaching condition, while ℓ_2 and ρ are selected to shape the fixed-time convergence rate. The parameter κ and the nonlinear shaping parameters (a, b) influence the sliding dynamics and transient response, whereas the barrier gain η controls the strength of constraint enforcement.

The final parameter values used in the experiments are: $\kappa = 0.005$, $a = 10$, $b = 0.1$, $\ell_1 = 0.1$, $\ell_2 = 0.1$, and $\rho = 1.5$.

A. Parameter tuning considerations: Although these values correspond to a specific experimental configuration, the tuning procedure follows general principles that can be adapted to different operating conditions. In particular, increasing ℓ_1 improves robustness to disturbances, while ℓ_2 and ρ influence the convergence speed. The parameters κ, a, and b affect the nonlinear sliding dynamics, allowing a trade-off between convergence rate and control effort, and η can be adjusted depending on the strictness of constraint enforcement.

To evaluate performance, six representative road profiles were used (Fig. 7):

- *Sinusoidal:* 3 Hz, 5 mm amplitude;
- *ISO B-Class:* filtered random road noise;
- *Pothole:* localized depression (5 mm depth, 2 s width);
- *Bump:* localized elevation (5 mm height, 2 s width);
- *Step:* +5 mm road step (sustained);
- *Frequency sweep:* 0.5–5 Hz, 3 mm amplitude.

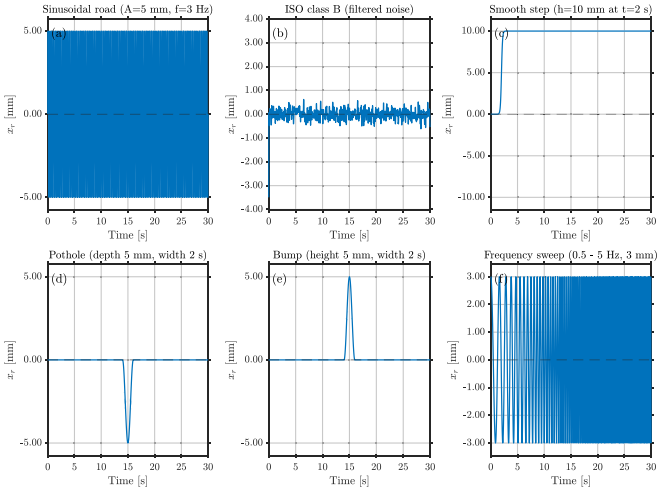

FIGURE 7. Road input profiles used for evaluation.

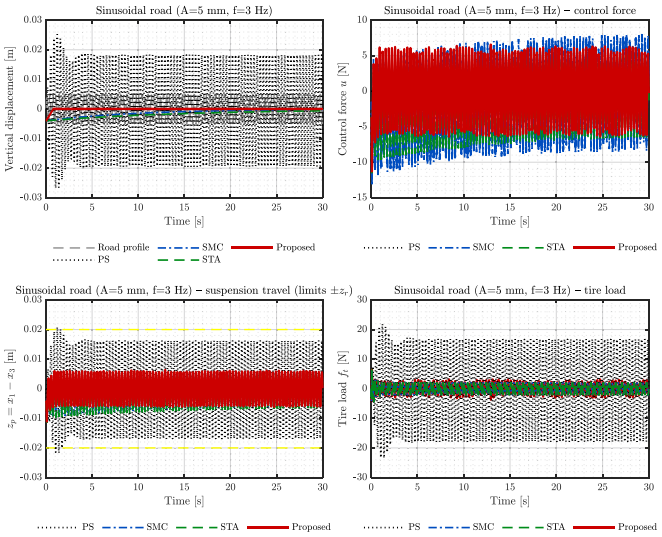

FIGURE 8. Performance on sinusoidal road (A=5 mm, f=3 Hz): top-left x_s (with road input), top-right u, bottom-left z_p with limits $\pm z_r$, bottom-right tire load f_t.

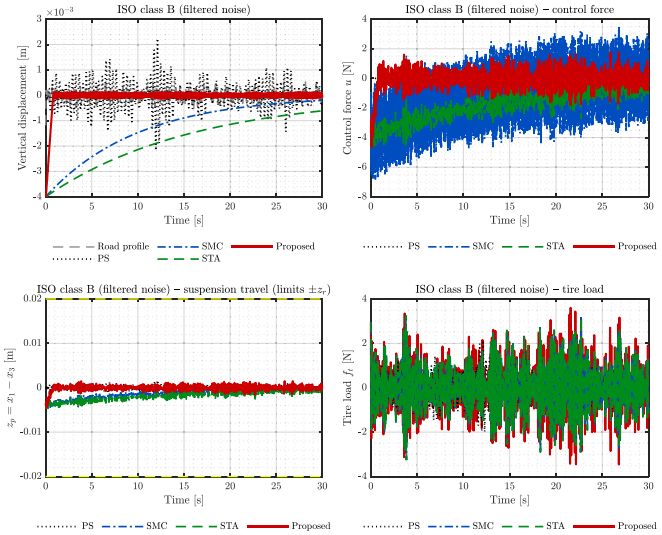

FIGURE 9. Performance on ISO class B (filtered noise). Panels as in Fig. 8.

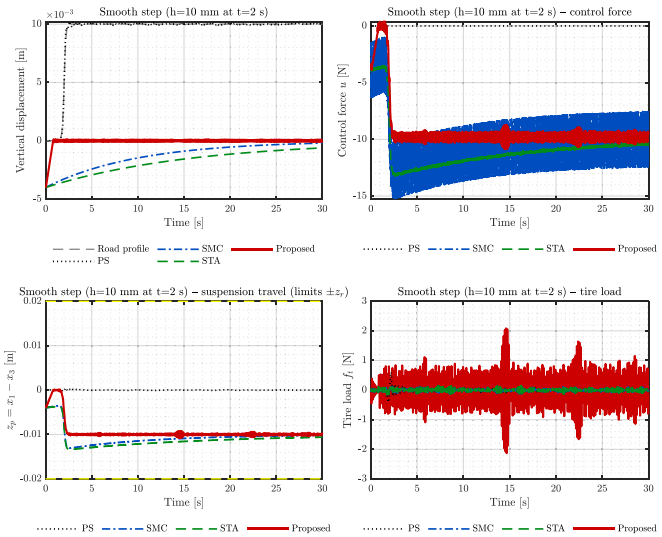

FIGURE 10. Performance on smooth step ($h = 10$ mm at $t = 2$ s). Panels as in Fig. 8.

Additionally, a matched disturbance $\Delta(t)$ was introduced to represent unmodeled dynamics and noise:

$$\Delta(t) = 0.01\sin(2\pi \cdot 0.5\,t) + 0.003\,\xi(t),$$

with $\xi(t)$ denoting Gaussian white noise, following common practice [3], [13], [44].

C. PERFORMANCE EVALUATION

The proposed fixed–time SMC controller (*FxT-SMC*) is evaluated against PS, SMC, and STA on six representative road inputs. For each profile, Figs. 8 –13 report the sprung–mass displacement x_s, the control force u, the suspension travel z_p with limits $\pm z_r$, and the tire load f_t. Quantitative indicators of comfort and constraint satisfaction are summarized in Table 3. The system is operated under explicit constraints $|z_p| \le z_r = 0.02\,\text{m}$ and $|f_t| \le 33\,\text{N}$, and all results below are interpreted with respect to these bounds. *A key distinction is convergence: FxT–SMC guarantees fixed–time convergence—experimentally within a short, profile–independent bound—whereas classical SMC and STA exhibit only asymptotic convergence.* The overall trend is consistent across all experiments: *FxT-SMC* delivers very low RMS and VDV with a nearly constant crest factor around 1.7, keeps z_p inside the allowed band, and avoids impulsive tire–load peaks.

On the sinusoidal road (3 Hz, 5 mm), *FxT-SMC* substantially improves ride comfort relative to PS. RMS acceleration decreases from $3.6418\,\text{m/s}^2$ (PS) to $0.0966\,\text{m/s}^2$, while VDV drops from $9.4773\,\text{m/s}^{1.75}$ to $0.2468\,\text{m/s}^{1.75}$. The crest factor remains low at 1.76, yielding a *Very Comfortable* (VC) classification. *In time domain, FxT–SMC settles to a small neighborhood of the origin in about 1 s on this periodic input, independent of the excitation phase.* The time

TABLE 3. Performance Summary Across Tested Road Profiles (Cft: VC=Very Comfortable, C=comfortable, UC=Uncomfortable, EUC=Extremely Uncomfortable)

Profile	Ctrl	RMS (m/s^2)	VDV ($m/s^{1.75}$)	CF (-)	Cft	$RMSE_x$ (m)	Max f_t (N)	Max z (m)
Sinusoidal	PS	3.6418	9.4773	1.79	EUC	1.34e-02	23.48	0.0217
	SMC	0.0022	0.0088	16.73	EUC	1.63e-03	6.45	0.0115
	STA	0.0021	0.0071	9.56	C	2.04e-03	6.44	0.0115
	Proposed	0.0966	0.2468	1.76	VC	3.92e-04	6.48	0.0111
ISO-B	PS	0.1473	0.5770	8.77	VC	5.01e-04	13.46	0.0029
	SMC	0.0022	0.0088	16.73	EUC	1.63e-03	13.46	0.0074
	STA	0.0021	0.0071	9.63	C	2.04e-03	13.46	0.0074
	Proposed	0.0965	0.2478	1.74	VC	3.96e-04	13.46	0.0072
Step	PS	0.0157	0.0675	8.10	VC	9.65e-03	0.61	0.0005
	SMC	0.0022	0.0088	16.73	EUC	1.63e-03	0.17	0.0131
	STA	0.0021	0.0071	9.55	C	2.04e-03	0.17	0.0134
	Proposed	0.0974	0.2469	1.68	VC	3.95e-04	2.14	0.0108
Pothole	PS	0.0127	0.0394	4.39	VC	8.04e-04	0.16	0.0001
	SMC	0.0022	0.0088	16.73	EUC	1.63e-03	0.18	0.0041
	STA	0.0021	0.0071	9.55	C	2.04e-03	0.18	0.0040
	Proposed	0.0968	0.2482	1.73	VC	3.97e-04	1.59	0.0051
Bump	PS	0.0123	0.0381	4.66	VC	8.01e-04	0.15	0.0001
	SMC	0.0022	0.0088	16.73	EUC	1.63e-03	0.17	0.0059
	STA	0.0021	0.0071	9.55	C	2.04e-03	0.17	0.0066
	Proposed	0.0969	0.2478	1.68	VC	3.96e-04	2.34	0.0051
Frequency sweep	PS	1.5427	5.6717	3.99	UC	7.14e-03	24.20	0.0218
	SMC	0.0022	0.0088	16.73	EUC	1.63e-03	7.50	0.0095
	STA	0.0021	0.0071	9.61	C	2.04e-03	7.50	0.0095
	Proposed	0.0966	0.2469	1.70	VC	3.91e-04	7.50	0.0091

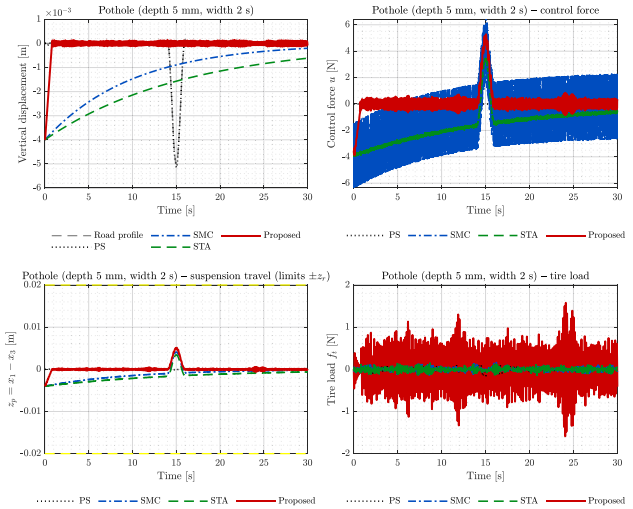

FIGURE 11. Performance on pothole (depth 5 mm, width 2 s). Panels as in Fig. 8.

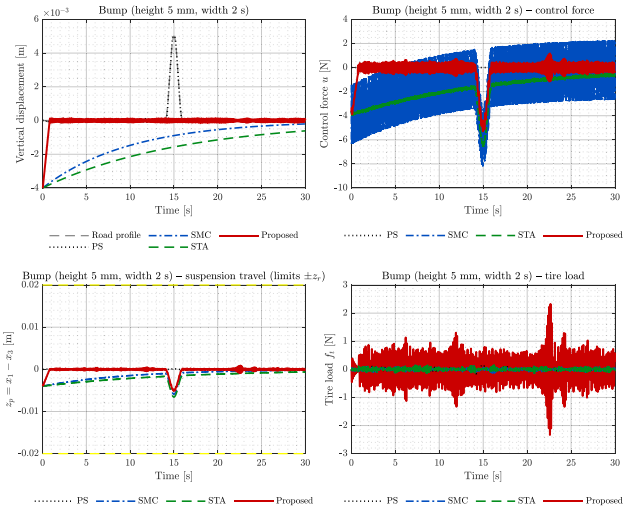

FIGURE 12. Performance on bump (height 5 mm, width 2 s). Panels as in Fig. 8.

histories in Fig. 8 show that z_p stays within bounds (Max $z = 0.0111\,\text{m} < 0.02\,\text{m}$) and that peak tire load is moderate (Max $f_t = 6.48\,\text{N} < 33\,\text{N}$). Although SMC and STA achieve small RMS on this input, their crest factors are large (CF $= 16.73$ and 9.56, respectively), which produces narrow, undesirable peaks and degrades comfort (EUC for SMC, C for STA). *Their trajectories approach equilibrium only asymptotically.*

Under ISO–B filtered noise, *FxT-SMC* maintains VC with RMS $0.0965\,\text{m/s}^2$, VDV $0.2478\,\text{m/s}^{1.75}$, and CF 1.74. Fig. 9 displays smooth u and f_t, and a z_p signal that remains well within $\pm z_r$ (Max $z = 0.0072\,\text{m} < 0.02\,\text{m}$). The largest tire-load excursion observed for *FxT-SMC* across all profiles occurs here (Max $f_t = 13.46\,\text{N}$), which still satisfies the $|f_t| \le 33\,\text{N}$ constraint with ample margin. *Despite the broadband disturbance, the FxT–SMC trajectories converge within roughly 1 to 1.5 seconds, whereas SMC/STA remain asymptotic.* In contrast, SMC exhibits a very high crest factor (CF $= 16.73$), visible as spiky transients in u and f_t, leading to an EUC rating despite a low RMS; STA remains Comfortable.

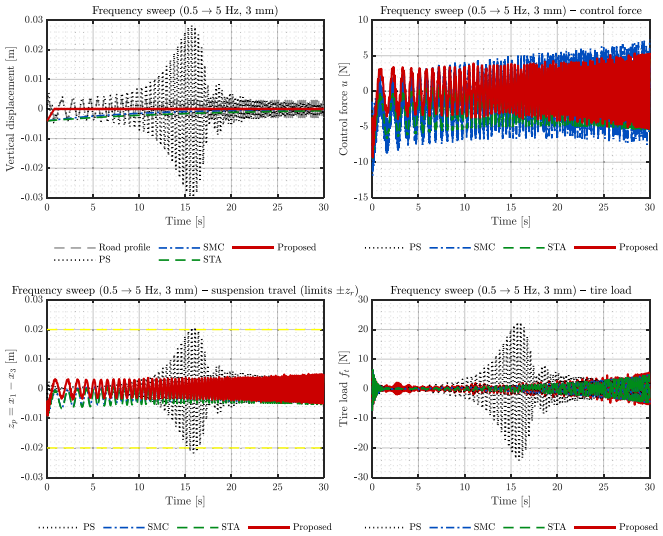

FIGURE 13. Performance on frequency sweep (0.5 → 5 Hz, 3 mm). Panels as in Fig. 8.

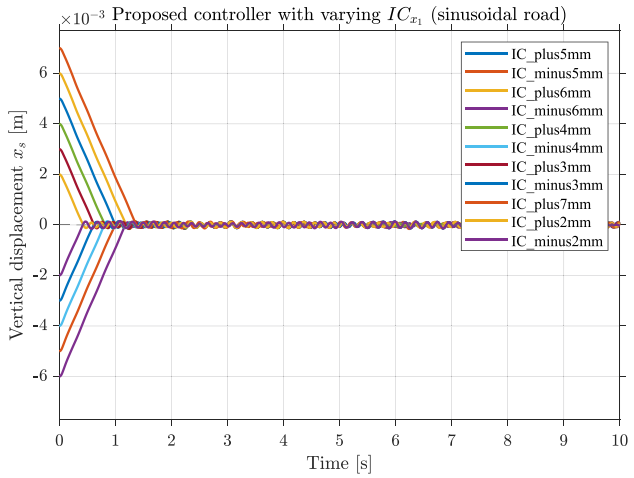

FIGURE 14. Sprung-mass displacement under $IC_{x_1} \in \{\pm 2, \pm 3, \pm 4, \pm 5, \pm 6, +7\}$ mm on a 3 Hz/5 mm sinusoidal road using the Proposed controller.

For the smooth step input ($h = 10$ mm at $t = 2$ s), *FxT-SMC* removes the low–frequency transient rapidly and yields a small tracking error ($\mathrm{RMSE}_x = 3.95 \times 10^{-4}$ m) without violating the travel constraint (Max $z = 0.0108$ m < 0.02 m); the control signal is well shaped and chatter–free. The resulting metrics (RMS 0.0974 m/s^2, VDV 0.2469 m/s$^{1.75}$, CF 1.68) confirm a VC level, as illustrated in Fig. 10. *Following the step at $t = 2$ s, the post-step transient is suppressed in well under 1 s,* and tire-load peaks remain moderate (Max $f_t = 2.14$ N < 33 N).

On localized defects, namely the pothole (depth 5 mm, width 2 s) and the bump (height 5 mm, width 2 s), the response with *FxT-SMC* is quickly damped and the suspension constraint is respected (Max $z \leq 0.0051$ m < 0.02 m). Comfort remains VC with crest factors near 1.7. *The disturbance-induced transients decay in about 1 s,* while peak tire loads rise relative to PS (e.g., 1.59 N on the pothole and 2.34 N on the bump) as the controller actively attenuates the disturbance—yet they stay far below the 33 N limit (see Figs. 11 and 12).

TABLE 4. Robustness to Initial Conditions for the FxT-SMC Controller on a Sinusoidal Road (3 Hz, 5 mm)

IC label	RMS [m/s^2]	VDV [m/s$^{1.75}$]	CF [–]	Cft	RMSE$_x$ [m]	Max f_t [N]	Max z [m]
IC_plus5mm	0.0917	0.1816	1.83	VC	9.38e-04	6.36	0.0101
IC_minus5mm	0.0924	0.1830	1.79	VC	9.25e-04	6.47	0.0121
IC_plus6mm	0.0917	0.1829	1.77	VC	1.22e-03	6.37	0.0111
IC_minus6mm	0.0917	0.1825	1.83	VC	1.20e-03	6.45	0.0131
IC_plus4mm	0.0933	0.1832	1.73	VC	6.82e-04	6.36	0.0091
IC_minus4mm	0.0935	0.1842	1.82	VC	6.72e-04	6.48	0.0111
IC_plus3mm	0.0945	0.1855	1.77	VC	4.56e-04	6.35	0.0081
IC_minus3mm	0.0945	0.1855	1.70	VC	4.47e-04	6.49	0.0101
IC_plus7mm	0.0908	0.1815	1.76	VC	1.52e-03	6.38	0.0121
IC_plus2mm	0.0960	0.1868	1.66	VC	2.62e-04	6.34	0.0071
IC_minus2mm	0.0930	0.1818	1.76	VC	2.56e-04	6.50	0.0091

During the frequency sweep (0.5→5 Hz, 3 mm), *FxT-SMC* preserves VC throughout the band with RMS 0.0966 m/s^2, VDV 0.2469 m/s$^{1.75}$, and CF 1.70, while PS becomes Uncomfortable as the excitation traverses the body–sensitive range (RMS 1.5427 m/s^2, VDV 5.6717 m/s$^{1.75}$); see Fig. 13. Suspension travel and tire load remain centered and bounded for *FxT-SMC* across the entire sweep (Max $z = 0.0091$ m $<$ 0.02 m, Max $f_t = 7.50$ N < 33 N). *Local transients induced by the changing excitation frequency dissipate on the order of 1 s, preserving a uniform fixed-time settling behavior across the band.*

Overall, across all six profiles *FxT-SMC* (i) consistently reduces RMS and VDV relative to PS while avoiding the excessive crest–factor spikes that penalize SMC, (ii) satisfies the travel constraint $|z_p| \leq z_r = 0.02$ m in every test, and (iii) bounds tire–load excursions with substantial margin to the $|f_t| \leq 33$ N limit, without inducing secondary oscillations. *Crucially, these behaviors are achieved with fixed–time convergence (sub-2-second settling across all cases, typically near 1 s), unlike the asymptotic convergence of SMC and STA.* These results meet the stated objective of improving ride comfort under explicit constraints with smooth, implementable control action, as corroborated by Table 3 and Figs. 8–13. All results reported above use the same initial condition for the sprung–mass state, $x_1(0) = \mathrm{IC}_{x_1} = -4 \times 10^{-3}$ m. The next subsection examines robustness by sweeping IC_{x_1} around this value and reporting the resulting trajectories and performance table.

D. ROBUSTNESS EVALUATION

Fig. 14 and Table 4 assess the robustness of the proposed fixed–time controller (*FxT–SMC*) to variations of the initial sprung–mass deflection, with $IC_{x_1} \in \{\pm 2, \pm 3, \pm 4, \pm 5, \pm 6, +7\}$ mm on a 3 Hz/5 mm sinusoidal input. For every initial offset, the *FxT–SMC* trajectories of x_s converge to a small steady oscillation within ≈ 1.5 s (uniform fixed-time settling), while preserving smooth control action. Comfort and constraint metrics show negligible sensitivity to the initial shift: RMS ranges from 0.0908 to 0.0960 m/s^2, VDV from 0.1815 to 0.1868 m/s$^{1.75}$, and the crest factor stays in 1.66–1.83, yielding a *Very Comfortable* rating

for all cases. Position-tracking accuracy is maintained with $\mathrm{RMSE}_x \in [2.56 \times 10^{-4},\ 1.52 \times 10^{-3}]$ m. Physical limits are respected with ample margins across all tests: the suspension travel remains below $\max|z_p| = 0.0131\ \mathrm{m} < z_r = 0.02$ m, and the tire load is bounded by $\max|f_t| = 6.50\ \mathrm{N} < 33$ N (headroom 80.3%). Taken together, these results indicate that *FxT–SMC* maintains its comfort level, enforces $|z_p| \le z_r$, and keeps tire–road contact forces low—even when the suspension is initialized several millimeters away from its nominal position—while guaranteeing fixed-time convergence of the transients.

VI. CONCLUSION

This paper introduced a continuous, non-singular fixed-time sliding-mode controller (FxT–SMC) for a nonlinear quarter-car active suspension subject to explicit suspension-travel constraints. By integrating a state-dependent fixed-time sliding map with a smooth reciprocal barrier defined on the normalized suspension deflection, the proposed framework ensures uniform fixed-time convergence with an initial-condition-independent settling-time bound, while preserving forward invariance of the admissible constraint set. The resulting control law remains continuous and implementable, mitigating chattering effects typically associated with conventional sliding-mode designs. Extensive evaluations over representative road profiles demonstrated consistent improvements in ISO 2631-1 comfort metrics, reduced crest-factor amplification, and strict enforcement of suspension-travel and tire-load limits. Robustness against variations in initial sprung-mass deflection further confirmed the transient predictability and reliability of the proposed approach. These results indicate that fixed-time, constraint-aware sliding-mode synthesis provides a viable pathway toward convergence-certified intelligent active suspension systems. Future work will address mismatched disturbances through dynamic extension and composite/robust observer structures while preserving fixed-time guarantees. Additional directions include Lyapunov-constrained reinforcement learning for adaptive gain tuning aimed at further reducing control effort and energy consumption, and the extension from fixed-time to predefined-time convergence so that the settling time can be explicitly prescribed under hard vehicular constraints.

APPENDIX A
CALCULUS IDENTITIES USED IN THE PROOF

Throughout, let

$$\psi(x_1) = |x_1|^{\frac{ax_1^2}{1+bx_1^2}} \operatorname{sgn}(x_1), \tag{30}$$

$$w = \frac{x_1 - x_3}{z_r}, \tag{31}$$

$$\Phi(w) = \frac{w}{1 - w^2}, \tag{32}$$

with $a, b, z_r > 0$.

A1 DERIVATIVE OF $\psi(x_1)$

For $x_1 \neq 0$, the derivative is given by the following expression, which is valid almost everywhere along system trajectories:

$$\psi(x_1) = \exp(p(x_1)\ln|x_1|)\operatorname{sgn}(x_1), \tag{33}$$

where

$$p(x_1) = \frac{ax_1^2}{1 + bx_1^2}, \tag{34}$$

$$p'(x_1) = \frac{2ax_1}{(1 + bx_1^2)^2}. \tag{35}$$

Using product and chain rules,

$$\frac{d\psi}{dx_1} = \operatorname{sgn}(x_1)\,|x_1|^{p(x_1)}\left(p'(x_1)\ln|x_1| + \frac{p(x_1)}{|x_1|}\right), \tag{36}$$

for a.e. $x_1 \neq 0$.

Multiplying by $\dot{x}_1 = x_2$ yields

$$\dot{\psi}(x_1) = \frac{a\,|x_1|\,x_2}{1 + bx_1^2}\left(1 + \frac{2\ln|x_1|}{1 + bx_1^2}\right)|x_1|^{\frac{ax_1^2}{1+bx_1^2}}. \tag{37}$$

It is important to note that although the analytical expression involves the term $\ln|x_1|$, which is not defined at $x_1 = 0$, the overall nonlinear term remains well-defined near the origin. In particular,

$$\lim_{x_1 \to 0} |x_1|\ln|x_1| = 0,$$

which ensures that the expression of $\dot{\psi}(x_1)$ does not introduce any singular behavior in the closed-loop dynamics.

A2 BARRIER TERM DERIVATIVES

For $w = \frac{x_1 - x_3}{z_r}$ and $\Phi(w) = \frac{w}{1-w^2}$,

$$\Phi'(w) = \frac{1 + w^2}{(1 - w^2)^2}, \tag{38}$$

$$\dot{w} = \frac{x_2 - x_4}{z_r}, \tag{39}$$

$$\Phi'(w)\dot{w} = \frac{1 + w^2}{(1 - w^2)^2}\,\frac{x_2 - x_4}{z_r}. \tag{40}$$

APPENDIX B
REGULARITY NOTE (NON-SMOOTH POINTS)

The nonlinear map

$$\psi(x_1) = |x_1|^{\frac{ax_1^2}{1+bx_1^2}} \operatorname{sgn}(x_1)$$

is continuous on $\mathbb{R}$ and satisfies $\psi(0) = 0$. Although its derivative involves the term $\ln|x_1|$, which is not defined at the origin, this does not lead to a true singularity in the closed-loop system.

Indeed, the apparent singularity is compensated by the multiplicative factor $|x_1|$, since

$$\lim_{x_1 \to 0} |x_1| \ln |x_1| = 0,$$

which guarantees that the nonlinear terms remain bounded in a neighborhood of the origin.

The time derivatives are therefore interpreted in the Filippov/Clarke sense for absolutely continuous solutions. Identities such as (37) hold almost everywhere in time, and the set $\{t : x_1(t) = 0\}$ has Lebesgue measure zero for generic trajectories.

Consequently, the Lyapunov-based fixed-time stability analysis remains valid, since it relies on differential inequalities that hold almost everywhere in time rather than on pointwise differentiability at $x_1 = 0$.

REFERENCES

[1] L. Ovalle, H. Rıós, and H. Ahmed, "Robust control for an active suspension system via continuous sliding-mode controllers," *Eng. Sci. Technol., Int. J.*, vol. 28, Apr. 2022, Art. no. 101026.

[2] R. Fattah, J. P. Kenne, K. Benjelloun, and A. Chebak, "Optimization of the backstepping control parameters of an active electrohydraulic suspension to improve passenger comfort and road handling," *IEEE Access*, vol. 13, pp. 35985–36005, 2025.

[3] Z. Zhou, M. Zhang, D. Navarro-Alarcon, and X. Jing, "Model-free finite-time saturated control for active vehicle suspension systems with dead zones and external disturbances," *Mech. Syst. Signal Process.*, vol. 229, Apr. 2025, Art. no. 112542.

[4] G. Chen, G. Du, J. Xia, X. Xie, and Z. Wang, "Aperiodic sampled-data H_∞ control of vehicle active suspension system: An uncertain discrete-time model approach," *IEEE Trans. Ind. Informat.*, vol. 20, no. 4, pp. 6739–6750, Apr. 2024.

[5] M. Yu, S. A. Evangelou, and D. Dini, "Advances in active suspension systems for road vehicles," *Engineering*, vol. 33, pp. 160–177, 2024.

[6] J. J. Rath, M. Defoort, C. Sentouh, H. R. Karimi, and K. C. Veluvolu, "Output-constrained robust sliding mode based nonlinear active suspension control," *IEEE Trans. Ind. Electron.*, vol. 67, no. 12, pp. 10652–10662, Dec. 2020.

[7] C. Kurz, L. Stangenberg, and F. Gauterin, "A generic approach to modeling vehicle pitch dynamics on a vehicle test bench," *IEEE Open J. Veh. Technol.*, vol. 4, pp. 739–748, 2023.

[8] V. Beliautsou et al., "Geographically distributed test environment: Validation of integrated motion control of multi-actuated electric vehicle," *IEEE Open J. Veh. Technol.*, vol. 6, pp. 1661–1672, 2025.

[9] R. Marotta et al., "Enhancing wheel vertical displacement estimation in road vehicles through integration of model-based estimator with artificial intelligence," *IEEE Open J. Veh. Technol.*, vol. 5, pp. 979–989, 2024.

[10] W. Cheng, T. Yin, and Z. Gu, "Memory-based dynamic event-triggered secure control of active suspension systems against deception attacks," *ISA Trans.*, vol. 165, pp. 64–71, 2025.

[11] H. Chen, M.-D. Gong, D.-X. Zhao, W.-B. Liu, and G.-Y. Jia, "Coordination control of multi-axis steering and active suspension system for high-mobility emergency rescue vehicles," *Mathematics*, vol. 10, no. 19, 2022, Art. no. 3562.

[12] R. Fattah, J.-P. Kenne, K. Benjelloun, and A. Chebak, "Optimization of sliding mode control parameters to improve passenger comfort, road handling and reduce chattering in active electrohydraulic suspension systems," in *Proc. 2025 Int. Conf. Control, Automat. Diagnosis*, 2025, pp. 1–6, [Online]. Available: https://ieeexplore.ieee.org/document/11099178/

[13] T. Shang, J. Zhang, and J. Long, "An adaptive neural network sliding mode controller for nonlinear active suspension with uncertain parameters and non-ideal actuators," May 2023. [Online]. Available: https://www.researchsquare.com/article/rs-2918883/v1

[14] J. Matute, S. Diaz, and A. Karimoddini, "Sliding mode control for robust path tracking of automated vehicles in rural environments," *IEEE Open J. Veh. Technol.*, vol. 5, pp. 1314–1325, 2024.

[15] R. Fattah, J. P. Kenne, K. Benjelloun, and A. Chebak, "Comparative analysis of reaching laws in sliding mode control for electrohydraulic active suspension systems under complex road trajectories," in *Proc. 7th Int. Conf. Mechatron., Robot. Automat.*, 2024, pp. 1–9.

[16] U. S. Pusadkar, S. D. Chaudhari, P. D. Shendge, and S. B. Phadke, "Linear disturbance observer based sliding mode control for active suspension systems with non-ideal actuator," *J. Sound Vib.*, vol. 442, pp. 428–444, Mar. 2019.

[17] Q. Zeng and J. Zhao, "Adaptive switching event-triggered control for active suspension systems with acceleration performance constraint," *IEEE Trans. Intell. Transp. Syst.*, vol. 24, no. 8, pp. 8028–8037, Aug. 2023.

[18] G. Wang, M. Chadli, and M. V. Basin, "Practical terminal sliding mode control of nonlinear uncertain active suspension systems with adaptive disturbance observer," *IEEE/ASME Trans. Mechatron.*, vol. 26, no. 2, pp. 789–797, Apr. 2021.

[19] A. A. Wijaya, F. Yakub, S. S. Abdullah, R. Akmeliawati, S. Aljazzar, and I. Makoto, "Neuroadaptive natural logarithm sliding mode control for nonlinear active suspension systems," *IEEE Trans. Intell. Veh.*, vol. 9, no. 11, pp. 7110–7124, Nov. 2024.

[20] T. Wang, H. Zhang, and S. Sui, "Observer-based adaptive neural network event-triggered quantized control for active suspensions with actuator saturation," *Neurocomputing*, vol. 614, 2025, Art. no. 128770.

[21] Y. Zhao, Y. Zhang, L. Guo, S. Ding, and X. Wang, "Advances in machine learning-based active vibration control for automotive seat suspensions: A comprehensive review," *Mech. Syst. Signal Process.*, vol. 231, 2025, Art. no. 112645.

[22] M. Zhang and X. Jing, "Switching logic-based saturated tracking control for active suspension systems based on disturbance observer and bioinspired x-dynamics," *Mech. Syst. Signal Process.*, vol. 155, 2021, Art. no. 107611.

[23] J. Peng, X. Shi, and Y. Hu, "Robust decoupled sliding mode control for active suspension systems with prescribed tracking performance," *Control Theory Technol.*, vol. 23, no. 2, pp. 310–320, 2025.

[24] J. Na, Y. Huang, X. Wu, S.-F. Su, and G. Li, "Adaptive finite-time fuzzy control of nonlinear active suspension systems with input delay," *IEEE Trans. Cybern.*, vol. 50, no. 6, pp. 2639–2650, Jun. 2020.

[25] M. Zhang, X. Jing, W. Huang, and P. Li, "Saturated PD-SMC method for suspension systems by exploiting beneficial nonlinearities for improved vibration reduction and energy-saving performance," *Mech. Syst. Signal Process.*, vol. 179, 2022, Art. no. 109376.

[26] Z. Zhang, J. Zhang, H. Yin, B. Zhang, and X. Jing, "Bio-inspired structure reference model oriented robust full vehicle active suspension system control via constraint-following," *Mech. Syst. Signal Process.*, vol. 179, 2022, Art. no. 109368.

[27] X. Guo, J. Zhang, and W. Sun, "Robust saturated fault-tolerant control for active suspension system via partial measurement information," *Mech. Syst. Signal Process.*, vol. 191, 2023, Art. no. 110116.

[28] Z. Liu, Y. Si, and W. Sun, "Ride comfort oriented integrated design of preview active suspension control and longitudinal velocity planning," *Mech. Syst. Signal Process.*, vol. 208, 2024, Art. no. 110992.

[29] B. Huang, S. Zhang, Y. He, B. Wang, and Z. Deng, "Finite-time anti-saturation control for Euler–Lagrange systems with actuator failures," *ISA Trans.*, vol. 124, pp. 468–477, 2022.

[30] A. Polyakov, "Nonlinear feedback design for fixed-time stabilization of linear control systems," *IEEE Trans. Autom. Control*, vol. 57, no. 8, pp. 2106–2110, Aug. 2012.

[31] E. Moulay, V. Lechappe, E. Bernuau, and F. Plestan, "Robust fixed-time stability: Application to sliding-mode control," *IEEE Trans. Autom. Control*, vol. 67, no. 2, pp. 1061–1066, Feb. 2022.

[32] W. Yu, X. Yu, and H. Wang, "Sliding Modes: From asymptoticity, to finite time and fixed time," *Sci. China Inf. Sci.*, vol. 66, no. 9, 2023, Art. no. 190205.

[33] T. Huang, J. Wang, and H. Pan, "Approximation-free prespecified time bionic reliable control for vehicle suspension," *IEEE Trans. Autom. Sci. Eng.*, vol. 21, no. 4, pp. 5333–5343, Oct. 2024.

[34] Z. Zhou, M. Zhang, H. Liu, and X. Jing, "Fixed-time safe-by-design control for uncertain active vehicle suspension systems with nonlinear reference dynamics," *IEEE/ASME Trans. Mechatron.*, vol. 29, no. 5, pp. 3348–3359, Oct. 2024.

[35] M. Labbadi, G. P. Incremona, and A. Ferrara, "Design of an easy-to-implement fixed-time stable sliding mode control," *IEEE Contr. Syst. Lett.*, vol. 7, pp. 3313–3318, 2023.
[36] N. P. Nguyen, H. Oh, J. Moon, and Y. Kim, "Multivariable disturbance observer-based finite-time sliding mode attitude control for fixed-wing uavs under matched and mismatched disturbances," *IEEE Control Syst. Lett.*, vol. 7, pp. 1999–2004, 2023.
[37] L. Zuo and S. A. Nayfeh, "Low order continuous-time filters for approximation of the ISO 2631-1 human vibration sensitivity weightings," *J. Sound Vib.*, vol. 265, pp. 459–465, Aug. 2003.
[38] K. Azrah, R. Mirzaei, M. Poursadeghiyan, M. M. Baneshi, and M. H. Ebrahimi, "Evaluation of whole-body vibration exposure among urban metro drivers: Comparing ISO2631-1 and ISO2631-5 standards to evaluate exposure," *Health Scope*, vol. 7, May 2018, Art. no. e55928.
[39] K. Shao, K. Huang, S. Duan, S. Zhen, and F. Gao, "Modelling and dynamic analysis of vehicles based on discrete constraints," *Int. J. Veh. Des.*, vol. 75, no. 1-4, pp. 23–46, 2017.
[40] K. Huang, W. Xia, K. Shao, and H. Sun, "Adaptive sliding mode control for vehicle active anti-roll system based on property adjustable barrier function," *IEEE Trans. Intell. Veh.*, vol. 10, no. 5, pp. 3124–3133, May 2025.
[41] S. P. Bhat and D. S. Bernstein, "Finite-time stability of continuous autonomous systems," *SIAM J. Control Optim.*, vol. 38, no. 3, pp. 751–766, 2000.
[42] B. Tian, Z. Li, and Q. Zong, "A continuous multivariable finite-time control scheme for double integrator systems with bounded control input," *IEEE Trans. Autom. Control*, vol. 67, no. 11, pp. 6068–6073, Nov. 2022.
[43] A. Khanzadeh and I. Mohammadzaman, "Fixed-time integral sliding mode control design for a class of uncertain nonlinear systems based on a novel fixed-time stability condition," *Eur. J. Control*, vol. 69, 2023, Art. no. 100753.
[44] H. Pan, X. Jing, and W. Sun, "Robust finite-time tracking control for nonlinear suspension systems via disturbance compensation," *Mech. Syst. Signal Process.*, vol. 88, pp. 49–61, May 2017.

RACHID FATTAH (Member, IEEE) received the M.Sc. degree in mechanical engineering from the Mohammadia School of Engineering (EMI), Rabat, Morocco, in 2021, and the Aggregation degree in industrial sciences in 2022. He is currently working toward the Ph.D. (by Research) degree with Green Tech Institute (GTI)/Mohammed VI Polytechnic University (UM6P), Ben Guerir, Morocco. Since 2022, he has been an Education Fellow with GTI/UM6P. He also focuses on the development of innovative solutions in automotive engineering and control systems. His research interests include the design and control of electrohydraulic suspension systems, advanced control techniques, and optimization methods such as game theory and particle swarm optimization (PSO) to enhance road handling and passenger comfort.

JEAN-PIERRE KENNÉ received the bachelor's degree in mechanical engineering from the University of Douala, Douala, Cameroon, in 1984, and the M.Sc. and Ph.D. degrees in mechanical engineering from Polytechnique Montréal, Montréal, QC, Canada, in 1991 and 1998, respectively. In 1999, he was with Digital Control System Department, GEBO Canada, as a Project Manager. In 2000, he joined the Department of Mechanical Engineering École de Technologie Supérieure (ÉTS), Montréal, where he currently Teaches Courses in control theory, fluid power systems, and the design and control of manufacturing systems. He is also a Professor with the Department of Mechanical Engineering and the Director with the Laboratory of Integrated Production Technologies. His research interests include control theory, capacity planning, control of manufacturing systems, and optimization of production systems.

KHALID BENJELLOUN received the State Engineer degree from the Mohammadia School of Engineering (EMI), Rabat, Morocco, in 1987, and the M.Sc.A. and Ph.D. degrees in mechanical engineering from Polytechnique Montréal, Montréal, QC, Canada, in 1993 and 1996, respectively. In 1989, he joined the Mohammadia School of Engineering, where he is currently a Professor teaching control theory, nonlinear control systems, and robotics. He is currently an affiliated Professor with the Green Tech Institute (GTI)/Mohammed VI Polytechnic University (UM6P), Ben Guerir, Morocco. His research interests include advanced, intelligent, nonlinear, and stochastic control systems, with applications in industrial processes, robotics, and systems with nonlinear and random dynamics.

AHMED CHEBAK (Senior Member, IEEE) received the M.Sc. and Ph.D. degrees from Laval University, Quebec, QC, Canada, and the Engineering Diploma degree in electromechanics from the National School of Mineral Industry, Rabat, Morocco. Since 2019, he has been a Professor of electrical engineering with Mohammed VI Polytechnic University, Morocco, and the Director with Green Tech Institute. He was a Full Professor with the University of Quebec, Rimouski, Canada, and a Research Associate and Lecturer with Laval University. His research interests include smart energy management, electric and hybrid vehicle traction system optimization, and electric machine design.